

Stringent Constraints on New Pseudoscalars from Precision Hyperfine Splitting Measurements

Cedric Quint,¹ Fabian Heiße,¹ Joerg Jaeckel,² Lutz Leimenstoll,² Christoph H. Keitel,¹ and Zoltán Harman¹

¹*Max Planck Institute for Nuclear Physics,
Saupfercheckweg 1, 69117 Heidelberg, Germany*

²*Institute for Theoretical Physics,
Philosophenweg 16, 69120 Heidelberg, Germany*

Axion-like particles and similar new pseudoscalar bosons coupled to nucleons and electrons are predicted to lead to spin-dependent forces in atoms and ions. We argue that hyperfine structure measurements in the hydrogen- and lithium-like charge states are a sensitive probe to this effect. Employing specific differences of these splittings reduces uncertainties due to nuclear effects in hyperfine structure calculations and measurements. Using this, we show that existing measurements on Be provide competitive limits in the region $m_\phi \gtrsim 100$ keV, improving upon existing constraints by up to a factor of 8. We also find that future measurements on Cs and In have a further order of magnitude improved discovery potential when compared with existing bounds.

In recent years, there has been increasing interest in investigating physics beyond the standard model (SM) using the tools of precision atomic spectroscopy (cf. Refs. [1–11]) as well as similar approaches (cf. Refs. [12–17]). Notably, a recent review [18] highlighted the sensitivity of atomic systems to new physics-induced spin-dependent interactions. This motivates new physics searches enabled by the prediction that the exchange of new bosons also implies the existence of new forces and potentials [19, 20].

Much of the existing work on new physics constraints derived from such efforts is focused on light atoms or isotope shifts, since the available precision in both theory and experiment is much higher when compared to the standalone spectroscopy of heavier elements [5, 15]. But we will argue that highly charged ions can also play an important role, notably for pseudoscalars.

Generally speaking, the experimental approach best suited for investigating forces induced by new particles generically depends on the Lorentz structure of the interaction [19, 20]. In this Letter, we focus on pseudoscalar interactions, leading to a dipole-dipole interaction between the electron(s) and the nucleus. Pseudoscalars appear in a wide range of extensions to the SM; light variants with interactions that are suppressed by a large new physics scale are often called axions or axion-like particles (ALPs) (cf., e.g., [21–24] for reviews). This is motivated by their similarity to QCD axions that arise as a consequence of the Peccei-Quinn (PQ) solution to the strong charge parity (CP) problem in QCD [25–30] (cf. [31] for an overview of models). In field theory, such pseudoscalars arise as pseudo Nambu-Goldstone bosons of a broken axial symmetry. They can also arise in string theory scenarios [32–45]. They feature in solutions to various open problems in physics, most notably as a possible light dark matter (DM) candidate, cf., e.g. [36, 46–50]. Due to their pseudoscalar nature, interactions mediated by such a particle induce spin-spin couplings in atomic systems [19, 20]. Hence, they give rise to an additional contribution to the hyperfine structure (HFS) in such systems, thereby giving access to possible experimental signatures of this effect.

For higher masses, this interaction is expected to be short-ranged, making it more difficult to detect in experiments searching for new forces, and limits are typi-

cally weaker [18]. To get access to the $\sim (1 - 100)$ MeV range, choosing an element with a high nuclear charge Z is an intuitive step, resulting in a shorter mean distance between the bound electron and the nucleus. However, finite nuclear size effects become relevant with increasing Z , which implies that this choice comes with the cost of theoretical precision. We mitigate this loss of accuracy by considering specific differences of hyperfine splittings. These are weighted differences between the hyperfine splitting energy of lithium- and hydrogen-like ions, with the weighting factor defined such that the effects due to the magnetization distribution of the nucleus are largely suppressed [51]. The study of hyperfine splitting in both charge states has recently been enabled by experimental developments with stored and trapped ions in the high- Z [52] and low- Z [53] regimes. This treatment improves the bounds on the pseudoscalar coupling constants one can derive from such measurements, even for hydrogen and helium [18, 54]. However, this also results in a suppression of the new physics effects for hydrogen and helium. This suppression is less pronounced for medium to highly charged ions (HCI) that can thus yield competitive bounds on this pseudoscalar interaction: as we show below, in the high-mass regime, the bounds can be improved by more than one order of magnitude compared to the best previous results. Another advantage of highly charged ions is that, via the choice of the isotope, one can selectively constrain proton and neutron coupling constants.

Theory. – The hyperfine structure of hydrogen has a rich history in the study of relativistic and radiative corrections to the energy levels predicted by the Schrödinger equation. This topic has reached an impressive level of maturity, leading to astonishing precision in both theory and experiment [52, 53, 55–58]. The plethora of methods and tools that became available in recent decades has led to numerous insights into the details of hyperfine splitting in hydrogen- and lithium-like ions. The former can be encapsulated into the following parametrization of the ground-state hyperfine splitting of hydrogen-like ions [55]

$$\begin{aligned} \Delta E_{\text{H-like}} &= \frac{4}{3} \alpha (\alpha Z)^3 \frac{\mu}{\mu_N} \frac{m_e}{m_p} \frac{2I + 1}{2I} \frac{m_e}{(1 + \frac{m_e}{M})^3} \\ &\times (A_{1s}(\alpha Z)(1 - \delta_{1s})(1 - \varepsilon_{1s}) + x_{\text{rad}}^{1s}). \end{aligned} \quad (1)$$

Here, α is the fine-structure constant, Z the nuclear charge, m_e the electron mass, m_p the proton mass, μ the nuclear magnetic moment, μ_N the nuclear magneton, I the nuclear spin, and M the nuclear mass. Natural units, i.e., $\hbar = c = 1$ are used throughout this work. Moreover, $A_{1s}(\alpha Z)$ denotes the relativistic factor [59],

$$A_{1s}(\alpha Z) = \frac{1}{\gamma(2\gamma - 1)}, \quad (2)$$

where $\gamma = \sqrt{1 - (\alpha Z)^2}$. Furthermore, δ_{1s} is the nuclear charge distribution correction, and ε_{1s} the nuclear magnetization distribution correction (Bohr-Weisskopf (BW) correction). Finally, x_{rad}^{1s} denotes radiative corrections (cf. Refs. [55, 60, 61]).

For lithium-like ions, one can observe a similar structure in the hyperfine splitting contributions, with the addition of inter-electronic interaction contributions [55]

$$\begin{aligned} \Delta E_{\text{Li-like}} &= \frac{1}{6} \alpha(\alpha Z)^3 \frac{\mu}{\mu_N} \frac{m_e}{m_p} \frac{2I+1}{2I} \frac{m_e}{(1 + \frac{m_e}{M})^3} \\ &\times \left([A_{1s}(\alpha Z) + \frac{1}{Z} B(\alpha Z) + \dots] \right. \\ &\times \left. (1 - \delta_{2s})(1 - \varepsilon_{2s}) + x_{\text{rad}}^{2s} \right). \end{aligned} \quad (3)$$

Here, $A_{2s}(\alpha Z)$ denotes the relativistic factor for the 2s system, $B(\alpha Z)$ denotes the photon exchange contribution to first order, and x_{rad}^{2s} parametrizes the radiative corrections for the lithium-like system. Moreover, δ_{2s} and ε_{2s} again denote the nuclear charge distribution and BW correction, respectively. We want to highlight the fact that the photon exchange contributions are given in a $1/Z$ expansion, since every photon exchange provides a factor of α , and thus an overall factor of $1/Z$ in the usual $Z\alpha$ expansion of atomic properties.

We calculate the energy shift induced by the spin-dependent interaction between an electron and the nucleus. To interpret the coupling of the pseudoscalar to the nucleus, we use the single-particle Schmidt model [62]. In this model, the spin of a nucleus with an odd number of nucleons is due to the orbital motion and intrinsic spin of only one valence nucleon. The spins and orbital angular momenta of all other nucleons sum up to zero and do not contribute to the spin-dependent coupling. Hence, the electron couples to that valence nucleon only. This approximation implies that we model a spin- $\frac{1}{2}$ particle as carrying the spin of the whole nucleus [63]. Thus, we give the corresponding interaction Lagrangian as

$$\mathcal{L}_{\text{int}} = i \sum_{k=e,N} g_k \bar{\psi}_k \gamma^5 \psi_k \phi. \quad (4)$$

Here, ψ_k denotes the Dirac field of the electron e or nucleon $N \in \{n, p\}$, where n denotes the neutron, and p the proton. Moreover, g_k is the respective coupling constant of the pseudoscalar to the indexed particle, ϕ the pseudoscalar field, and γ^5 denotes the fifth Dirac gamma matrix. Using the non-relativistic approximation for the dynamics of the nucleon, one obtains the following potential from the aforementioned interaction

Lagrangian [54, 64]

$$V_\phi(r) = -i \frac{g_N g_e}{8\pi m_N} \boldsymbol{\sigma}_N \cdot \hat{\mathbf{r}} \frac{e^{-m_\phi r}}{r} (m_\phi + 1/r) \gamma^0 \gamma^5. \quad (5)$$

Here, r is the radial variable in the system of the nucleus, m_N and m_ϕ are the masses of the nucleon and the exchange boson, respectively, $\boldsymbol{\sigma}_N$ is the vector of Pauli matrices acting on the wave function of the nucleon, and $\hat{\mathbf{r}} = \mathbf{r}/r$ is the unit coordinate vector. In the following, the Pauli matrices are reinterpreted as $(2I+1)$ -dimensional spin operators acting on the nuclear spin states $|I, M_I\rangle$. Symbolically, this implies defining $\boldsymbol{\sigma}_N \rightarrow 2\mathbf{I}$ within the single-particle Schmidt-model. Employing the usual methods via the Wigner-Eckhart theorem, for e.g., hyperfine splitting calculations [65], we then obtain the following energy shift for the induced hyperfine splitting

$$\begin{aligned} \Delta E &= -\frac{g_N g_e}{8\pi} \frac{m_e^2}{m_N} (2I+1) \frac{1}{j(j+1)} \\ &\times \int_r \beta(r) F_{n,\kappa}(r) G_{n,\kappa}(r) dr. \end{aligned} \quad (6)$$

Here, j is the angular momentum quantum number of the electron. The functions F, G are small and large radial components of the Dirac-Coulomb wavefunctions obtained in the nuclear potential corresponding to the Fermi proton distribution (cf. Refs. [65, 66] and the Appendix). Moreover, we defined the potential function

$$\beta(r) = \frac{e^{-m_\phi r}}{r} (m_\phi + 1/r). \quad (7)$$

From this, the pseudoscalar-induced hyperfine structure becomes readily calculable in the one-electron approximation. For lithium-like ions, however, the interactions between electrons become relevant due to the overlap of the core and valence s electrons in the nuclear region. We treat this effect as discussed in Ref. [58], i.e., via the addition of screening terms to the nuclear potential and perturbation theory in α . The former approach is known as treating the system within the *extended Furry picture* [58, 67, 68]. To this end, we take the effective potential for the electrons in the lithium-like system to be the Kohn-Sham (KS) potential [69, 70] from density functional theory [68, 71],

$$V(r) = V_C(r) + V_{\text{KS}}(r) \quad (8)$$

where V_C denotes the Coulomb potential induced by the extended nucleus, α is the fine-structure constant and $V_{\text{KS}}(r)$ is the KS potential which is explicitly given in the Appendix. The KS potential is solely determined by the electron probability density around the nucleus. We obtain this density self-consistently via the wavefunctions from the Dirac-Hartree-Fock (DHF) procedure outlined in Ref. [72]. The hyperfine structure calculations are then carried out using radial wavefunctions that were obtained numerically by solving the Dirac equation with this modified potential term.

Up to first order in α , we consider the one-photon exchange contribution to the hyperfine splitting in the lithium-like system perturbatively. Schematically, this contribution is given by the following diagram:

$$(9)$$

where a double line denotes an electron propagating in the nuclear potential V , the wavy line represents the exchange of a photon, and the dashed line terminated by a square the pseudoscalar potential V_ϕ in Eq. (5). The second diagram denotes a counter-term contribution we add to avoid double-counting interaction effects when calculating the photon exchange contribution within the extended Furry picture. Hence, the white circle denotes an insertion of the screening potential, i.e., $V_C(r) - V(r)$. For details on this calculation, see the Appendix and Ref. [58].

With this approach, we have included the Coulomb interactions between electrons to high order by using a self-consistent screening potential and included relativistic corrections to the Coulomb repulsion up to first order by including the photon exchange contributions.

The observable we use to derive our constraints is the *specific difference* of HFS energies between lithium- and hydrogen-like systems of the same isotope. This weighted difference is constructed to suppress uncertainties originating from the BW effect [73].

These specific differences were first discussed for bismuth in Ref. [51], where it was shown that they can be calculated with significantly higher precision than the individual HFS contributions. They are defined as

$$\Delta'E = \Delta E_{\text{Li-like}} - \xi \Delta E_{\text{H-like}}. \quad (10)$$

Here, the factor ξ is defined as the ratio of the BW shifts of the respective systems, i.e.,

$$\xi = \frac{\Delta E_{\text{Li-like}}^{\text{BW}}}{\Delta E_{\text{H-like}}^{\text{BW}}}. \quad (11)$$

Since ξ itself can be obtained with much higher precision than the individual BW terms themselves, the resulting specific difference offers a robust observable with reduced theoretical uncertainty. For many elements, ξ is not readily tabulated in the literature. In such cases, we extract it by taking the ratio of the BW shifts from Ref. [74]. Whenever dedicated calculations of ξ exist, we use those values. We note that our bounds are not sensitive to variations of ξ beyond the fourth digit.

We compare our results with constraints derived from helium and hydrogen. For those elements, one can also define an alternative specific difference to suppress the nuclear effects in their hyperfine structure, known as D_{21} [1]. Here, one compares the hyperfine intervals of a $1s$ and excited $2s$ state

$$D_{21} = 8\Delta E_{2s} - \Delta E_{1s}, \quad (12)$$

where ΔE_{1s} is the $1s$ hyperfine splitting, and ΔE_{2s} corresponds to the respective $2s$ hyperfine splitting in H and alternatively $^3\text{He}^+$. We note an analogy to $\Delta'E$ when employing $\xi = 1/8$ (with different systems), which approximately holds for low- Z elements in general. In

Table I, we present the theory and experimental values for D_{21} in helium and hydrogen along with the values for $\Delta'E$ in heavier elements.

Results. – We give the results in an approach similar to Ref. [75], meaning we determine the 95% confidence interval (C.I.) for the difference between theory and experiment. We choose the parameters for the Gaussian as follows

$$\begin{aligned} \bar{x} &= |\text{Theory} - \text{Experiment}| \\ \sigma &= \sqrt{\sigma_{\text{theo}}^2 + \sigma_{\text{exp}}^2}. \end{aligned} \quad (13)$$

To set our constraints we use the “difference” between theory and experiment,

$$\delta E = \delta'E + \bar{x} \quad (14)$$

where we define $\delta'E$ by

$$95\% = \frac{1}{\sqrt{2\pi}\sigma} \int_{-\delta'E+\bar{x}}^{\delta'E+\bar{x}} e^{-\frac{(x-\bar{x})^2}{2\sigma^2}} dx, \quad (15)$$

to obtain quite conservative bounds. For the projections on caesium, indium, and xenon we assume $\bar{x} = 0$ and use estimates of the attainable theoretical and experimental uncertainties outlined in the Appendix.

Our bounds on the new pseudoscalar are then obtained via the condition

$$|\Delta E_{\text{Li-like}} - \xi \Delta E_{\text{H-like}}| \leq \delta E. \quad (16)$$

We also consider variation of the nuclear g -factor due to the effect of pseudoscalars in the corresponding measurement via the Zeeman splitting of hyperfine levels [80, 81]. Since the system of equations connecting the two measurements, i.e., the HFS and nuclear g -factor measurement, is not degenerate, we can disentangle the two. This is outlined in the Appendix. We find that taking this into account reproduces the constraints derived from Eq. (16). Alternatively, one may also obtain the nuclear g -factor from a measurement with a bare nucleus, avoiding the possibility of pseudoscalar effects being relevant entirely.

The limits on the pseudoscalar parameter space we obtain from Eq. (16) are shown in Fig. 1.

Future measurements with Cs and In promise to extend the sensitivity to the combination, $g_e g_p$, of a pseudoscalar-electron and pseudoscalar-proton coupling, by up to one order of magnitude for higher masses. Using Be as a probe already improves the sensitivity to couplings with neutrons, $g_e g_n$, by up to a factor of 8. We note the expected feature that heavier elements provide better bounds at higher masses due to the lower mean distance between the electrons and the nucleus. However, this is tempered by reduced theoretical and experimental precision. At low masses, the difference between bounds cannot be attributed to sensitivities alone. We also find that the strength of the constraint depends on the scaling of the specific difference, i.e., if the specific difference due to new physics scales similarly to the BW effect, the resulting bounds are less stringent. This is the case for hydrogen and

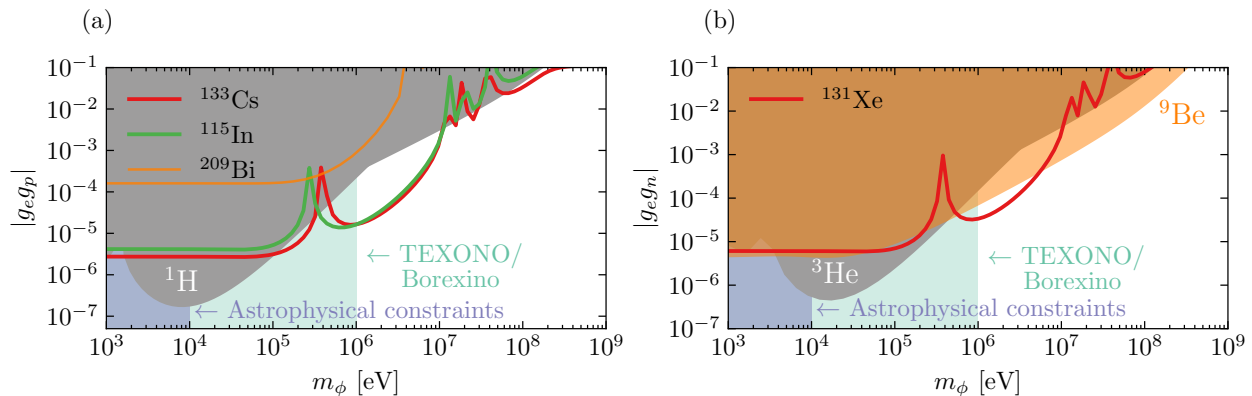


Figure 1. Bounds on the pseudoscalar parameter space resulting from hyperfine splitting & astrophysical observables. The left plot (a) shows bounds on the product of the electron & proton couplings, whereas the right one (b) shows the bounds on the product of electron & neutron couplings. Red, orange, and green lines (projections) and orange areas (current constraints) are bounds derived in this work. The gray area on the left (a) denotes bounds from the hydrogen specific difference D_{21}^H [75] and $1s$ hyperfine splitting [76]. The gray area on the right-hand side (b) denotes bounds from the helium-3 specific difference D_{21}^{He} and $1s$ HFS. The blue area in both plots denotes exclusions due to astrophysics we obtained from Ref. [18], while the green area shows TEXONO [77] and Borexino [78] bounds. Each bound derived in the present work is the most conservative bound considering the error we estimate by comparing our calculations with Ref. [58] (cf. Appendix for details). The bismuth constraint is a projection assuming that a future direct measurement of the nuclear magnetic moment will yield the NMR result found in the literature.

Table I. Values for ξ , I & the corresponding specific differences (D_{21} for helium & hydrogen, $\Delta'E$ for the rest) for different elements. TW indicates uncertainty estimates derived in this work (see the Appendix).

Element	I	ξ	Theory (meV)	Experiment (meV)	Refs.
^1H	1/2	0.125	$2.02458(10) \times 10^{-7}$	$2.02479(95) \times 10^{-7}$	[75]
^3He	1/2	0.125	$-4.9218(6) \times 10^{-6}$	$-4.92137(29) \times 10^{-6}$	[79]
^9Be	3/2	0.04881891046	$-1.224(15) \times 10^{-6}$	$-1.13581530(5) \times 10^{-6}$	[53]
^{115}In	9/2	0.13258	$\Delta'E_{\text{In}} \pm 7 \times 10^{-5}$	$\Delta'E_{\text{In}} \pm 1 \times 10^{-5}$	[74], TW
^{131}Xe	3/2	0.13660	$\Delta'E_{\text{Xe}} \pm 7 \times 10^{-5}$	$\Delta'E_{\text{Xe}} \pm 1 \times 10^{-5}$	[74], TW
^{133}Cs	7/2	0.13745	$\Delta'E_{\text{Cs}} \pm 7 \times 10^{-5}$	$\Delta'E_{\text{Cs}} \pm 1 \times 10^{-5}$	[74], TW
^{209}Bi	9/2	0.16885	$-61.043(35)$	$-61.012(26)$	[51, 52]

helium, where the scaling turns out to be almost identical. This is the suppression we mentioned in the introduction, indicating that heavier elements can indeed be better suited to derive such constraints despite the reduced sensitivities due to nuclear effects.

Said suppression can be attributed to the fact that the systems used to form the specific differences in helium and hydrogen do not include interelectronic interactions, which enables us to consider the following ratio

$$\frac{\int dr F_{2s}(r) G_{2s}(r) \beta(r)}{\int dr F_{1s}(r) G_{1s}(r) \beta(r)} \xrightarrow{m_\phi \rightarrow 0} \frac{1}{8} + \mathcal{O}((Z\alpha)^2), \quad (17)$$

implying (note that $\xi = 1/8$ for helium and hydrogen) that the new physics contributions in the hydrogen and helium specific differences cancel for low pseudoscalar masses up to relativistic corrections. Note that this may also happen for heavier elements depending on the value of the ratio ξ . However, this is not the case for the systems we consider, for which we have found that the missing suppression is not caused by computational inaccuracies.

We also note that the astrophysical constraints for the electron coupling may be extended to higher masses

by including the results from Ref. [82]. Yet, we also believe that the required supernova bound on the nucleons does not apply due to its falling into the trapping regime (cf. Ref. [83]), thereby weakening the bound.

Conclusions and Outlook. – In this Letter, we investigated bounds on new pseudoscalars using hyperfine splitting measurements of highly charged ions. We employed specific differences as a suitable observable, which enabled us to overcome limitations of the theoretical accuracy due to the Bohr-Weisskopf effect for the most part. This demonstrates that future precision spectroscopy of ions in the mid to high- Z regime will deliver competitive bounds on the pseudoscalar parameter space, improving upon existing constraints from hydrogen by up to a factor of 20.

This analysis of new physics induced atomic interactions via precise methods, both in theory and experiment, may be extended beyond the scope of our work by considering more interaction types and by increasing the accuracy via the inclusion of higher-order QED contributions to the observables of choice.

Acknowledgements. – C. Q. wishes to thank V. A. Yerokhin, N. S. Oreshkina, and L. Pütter for in-

sightful discussions. This work is supported by the Collaborative Research Centre 1225 funded by Deutsche Forschungsgemeinschaft (DFG, German Re-

search Foundation)–Project No. 273811115–SFB 1225. This article comprises parts of the PhD thesis work of C. Q. to be submitted to Heidelberg University.

Appendix

Considered systems, Hamiltonians & electron wave-functions. – We consider two different systems to obtain our bounds. The first system is the hydrogen-like ion, for which we use the following Hamiltonian

$$H_{\text{H-like}} = \boldsymbol{\alpha} \cdot \mathbf{p} + \beta m + V_{\text{C}}(r), \quad (18)$$

where α^i and β denote the corresponding Dirac matrices in the Dirac basis and V_{C} accounts for the Coulomb interaction. We model the Coulomb interaction as originating from a Fermi charge distribution [72, 84], i.e.,

$$\rho_{\text{C}}(r) = \frac{\rho_0}{1 - e^{-\frac{r-c}{a}}}, \quad (19)$$

where c is the half-density radius, and a can be given via the *skin-thickness* t as $a = 4 \ln 3 \cdot t$. This gives a constant value for a regardless of the element under consideration. The Hamiltonian for the lithium-like system is defined analogously as

$$H_{\text{Li-like}} = \boldsymbol{\alpha} \cdot \mathbf{p} + \beta m + V(r). \quad (20)$$

Here, $V(r) = V_{\text{KS}}(r) + V_{\text{C}}(r)$ includes screening effects via the Kohn-Sham potential

$$V_{\text{KS}}(r) = \alpha \int_{r>} \frac{\rho(r')}{r'} dr' - \frac{2\alpha}{3r} \left(r \rho(r) \frac{31}{82\pi^2} \right)^{1/3}, \quad (21)$$

with the probability density ρ encoding the screening effects due to the electrons present in the ion. This density is given by

$$\rho(r) = 2(\tilde{F}_{1s}(r)^2 + \tilde{G}_{1s}(r)^2) + (\tilde{F}_{2s}(r)^2 + \tilde{G}_{2s}(r)^2). \quad (22)$$

Here, the wavefunctions \tilde{F}, \tilde{G} were obtained self-consistently via the DHF procedure outlined in Ref. [72]. Aside from the aforementioned DHF procedure, the corresponding wavefunctions are obtained by solving the respective Dirac equations, whose general form is as follows

$$\psi_{n,\kappa,m}(r) = r^{-1} \begin{pmatrix} G_{n,\kappa}(r) \Omega_{\kappa,m}(\theta, \varphi) \\ i F_{n,\kappa}(r) \Omega_{-\kappa,m}(\theta, \varphi) \end{pmatrix}. \quad (23)$$

Here, F and G denote the radial wavefunctions for different parity states, whereas Ω denotes spherical spinors. The quantum number n denotes the usual primary quantum number, while $\kappa = \pm(j+1/2)$ is the relativistic angular momentum number, and m indicates the angular momentum projection. More information on these functions and their properties can be found in Ref. [66].

Connection to the non-relativistic result. – Although our treatment of the dynamics of the bound electrons is fully relativistic, it is useful to see if our calculations reduce to the known non-relativistic results found in the literature [19, 82]. To this end, we investigate the non-relativistic case as follows: for brevity's sake, consider simplified wave functions of the type

$$\psi = \begin{pmatrix} \varphi_1 \\ \varphi_2 \end{pmatrix}, \quad (24)$$

where φ_1 denotes the large, and φ_2 the small component of the *full* Dirac spinor shown in Eq. (23). In the non-relativistic limit, i.e., $E \approx m_e$ and $Z\alpha \ll 1$, one of the coupled Dirac-Coulomb equations simplifies to

$$-i\boldsymbol{\sigma}_e \cdot \nabla \varphi_1 - 2m_e \varphi_2 \approx 0. \quad (25)$$

This enables us to rewrite the full HFS matrix element using partial integration

$$\int d^3\mathbf{r} [-\varphi_2^\dagger \tilde{V} \varphi_1 + h.c.] = \frac{-i}{2m_e} \int d^3\mathbf{r} \varphi_1^\dagger (\boldsymbol{\sigma}_e \cdot \nabla \tilde{V}) \varphi_1, \quad (26)$$

where we used that the integrand vanishes on the boundary at infinity, and defined the following modified potential term

$$\tilde{V} = -i \frac{g_N g_e}{8\pi m_N} (\boldsymbol{\sigma}_N \cdot \nabla) \left(\frac{e^{-m_\phi r}}{r} \right). \quad (27)$$

Using this definition, we see that the procedure outlined above yields a new potential term within the integral. This new potential is given by [54]

$$i(\boldsymbol{\sigma}_e \cdot \nabla) \tilde{V} = \frac{g_N g_e}{16\pi m_e m_N} (\boldsymbol{\sigma}_e \cdot \nabla) (\boldsymbol{\sigma}_N \cdot \nabla) \left(\frac{e^{-m_\phi r}}{r} \right). \quad (28)$$

This matches the non-relativistic pseudoscalar-mediated potential usually found in the literature (cf. Ref. [19, 54]), confirming that our relativistic formulation is consistent with the non-relativistic approach.

Photon exchange & counter term diagrams. – Here, we give the algebraic expressions for the first-order interelectronic interaction diagrams. For a more thorough treatment and discussion of these contributions, one may refer to Refs. [58, 85].

The energy shift due to the one-photon exchange diagram is given by the following expression

$$\begin{aligned} \Delta E_{(1s)^2 2s, \gamma}^{(1)} = & \sum_b \sum_{m_a, M_I} \sum_{m'_a, M'_I} C_{j_a m_a, IM_I}^{FM_F} C_{j_a m'_a, IM'_I}^{FM_F} \langle IM'_I | \\ & \times \left[\sum_P (-1)^P (\langle \xi_b | P_a P_b | V_\phi | a \rangle + \langle \xi_a | P_b P_a | V_\phi | b \rangle) - \frac{1}{2} (\langle a | V_\phi | a \rangle + \langle b | V_\phi | b \rangle) \langle ab | I'(\varepsilon_a - \varepsilon_b) | ba \rangle \right] | IM_I \rangle, \end{aligned} \quad (29)$$

with the following identities

$$|\xi_a | P_b P_a \rangle = \sum_n |n\rangle \frac{\langle na | I(\Delta) | P_b P_a \rangle}{\varepsilon_b - \varepsilon_n} \quad \text{and} \quad |\xi_b | P_a P_b \rangle = \sum_n |n\rangle \frac{\langle nb | I(\Delta) | P_a P_b \rangle}{\varepsilon_a - \varepsilon_n}, \quad (30)$$

where P denotes the permutation operator, ε stands for the eigenenergies of the indexed states, and $|a\rangle = |j_a m_a\rangle$ represent electron states, with a being the valence ($2s$) state, and b denoting the core ($1s$) states, respectively. The states $|IM_I\rangle$ refer to the nuclear angular momentum states, which we couple to the valence electrons via the addition of angular momenta. Moreover, we denote the photon exchange operator as $I(\omega)$. It is defined as

$$I(\omega, r_{12}) = \alpha \frac{1 - \boldsymbol{\alpha}_1 \boldsymbol{\alpha}_2}{r_{12}} e^{i\sqrt{\omega + i0} r_{12}}, \quad (31)$$

in the Feynman gauge, with the arguments being $\Delta = \varepsilon_a - \varepsilon_{Pa}$, and $r_{12} = |\mathbf{r}_1 - \mathbf{r}_2|$. Finally, the contribution due to the counter term is given by


$$E_{(1s)^2 2s, \text{counter}}^{(1)} = 2 \sum_n \langle a | V_\phi | n \rangle \frac{\langle n | V_C(r) - V(r) | a \rangle}{\varepsilon_a - \varepsilon_n}, \quad (32)$$

where the factor of two arises as a symmetry factor due to the possible permutations of the diagram. We further suppressed the coupling to angular momentum in this contribution. This needs to be carried out analogously to the previous diagrams.

The effect of pseudoscalars on the measurement of the nuclear g_I -factor.— Determination of the Standard Model value of the specific differences requires the measured nuclear g_I -factor as an input. We therefore have to consider the possibility that this measurement, too, is affected by new physics contributions. One possibility to measure the nuclear g_I -factor is via a measurement of the g_F -factor, of a combined system, such as a hydrogen-like ion. The nuclear g_I -factor can then be extracted via a combined measurement of the Zeeman splitting of two hyperfine states (cf. Refs. [80, 81])

$$\bar{g} = g_{F=I+1/2} + g_{F=I-1/2} = -2 \frac{m_e}{m_p} g_I (1 - \sigma). \quad (33)$$

Here, the dimensionless term σ contains spin-dependent shielding corrections to the bound electron g -factor. In the presence of a new pseudoscalar, there are additional contributions to this quantity, given by the following diagram



$$, \quad (34)$$

where the wavy line terminated by a triangle denotes an insertion of the Zeemann potential induced by an

external magnetic field

$$V_{Zee}(r) = \frac{|e|}{2} \mathbf{B} \cdot (\mathbf{r} \times \boldsymbol{\alpha}). \quad (35)$$

In analogy to the QED case presented in Refs. [80, 81], this diagram induces an additional energy shift, given by

$$\begin{aligned} \Delta E = & 2 \sum_{n \neq a} \sum_{M_I, M'_I} \sum_{m_a, m'_a} C_{j_a m_a, IM_I}^{FM_F} C_{j_a m'_a, IM'_I}^{FM_F} \\ & \times C_{j_n m_n, IM''_I}^{FM_F} C_{j_n m'_n, IM'''_I}^{FM_F} \frac{1}{\varepsilon_a - \varepsilon_n} \\ & \times \langle IM'_I | \langle a | V_{Zee} | n \rangle | IM''_I \rangle \\ & \times \langle IM'''_I | \langle n | V_\phi | a \rangle | IM_I \rangle. \end{aligned} \quad (36)$$

For the measurements in question, we consider the specific case $j_a = 1/2$. The nuclear prefactors can then be factored out, giving the following expression for the pseudoscalar induced shielding contribution

$$\sigma_p = \frac{\Delta E}{M_F B \frac{\langle \mathbf{I} \cdot \mathbf{F} \rangle}{F(F+1)}}, \quad (37)$$

with the usual angular factor known from hyperfine splitting calculations

$$\langle \mathbf{I} \cdot \mathbf{F} \rangle = (F(F+1) - I(I+1) - j(j+1))/2, \quad (38)$$

where j denotes the electron spin, I denotes the nuclear spin, and F stands for the spin of the combined system. From this, we can see that the equation used to determine the nuclear g -factor is modified as

$$\bar{g}_p = \bar{g} + 2 \frac{m_e}{m_p} \sigma_p. \quad (39)$$

Similarly, we can write down the SM and new physics contributions to the specific difference of hyperfine splitting intervals. Considering both at the same time, we can connect the variation of both observables with the following system of equations

$$\begin{pmatrix} \delta(\Delta' E) \\ \delta \bar{g} \end{pmatrix} = \begin{pmatrix} \frac{\partial \Delta' E}{\partial g_I} & \frac{\partial \Delta' E}{\partial g_e g_N} \\ \frac{\partial \bar{g}}{\partial g_I} & \frac{\partial \bar{g}}{\partial g_e g_N} \end{pmatrix} \begin{pmatrix} \delta g_I \\ \delta(g_e g_N) \end{pmatrix}, \quad (40)$$

where $g_N \in \{g_n, g_p\}$ denotes either the neutron or proton coupling of the pseudoscalar. We find that the

matrix in the above equation is invertible within the mass range in which we derive our bounds, meaning we can disentangle the two measurements. Our bounds are then also obtained by solving the above system of equations (cf. also [2]), i.e.,

$$|\delta(g_e g_p)| \leq \frac{\left| \frac{\partial \Delta' E}{\partial g_I} \delta \bar{g} \right| + \left| \frac{\partial \bar{g}}{\partial g_I} \delta(\Delta' E) \right|}{\left| \frac{\partial \Delta' E}{\partial g_I} \frac{\partial \bar{g}}{\partial g_e g_N} - \frac{\partial \Delta' E}{\partial g_e g_N} \frac{\partial \bar{g}}{\partial g_I} \right|}. \quad (41)$$

We find that deriving the bounds this way reproduces the “naive” bounds obtained from Eq. (16), implying that we can indeed resolve the two measurements via the solution of the coupled system of equations. Thus, we conclude that the naive bounds derived from Eq. (16) apply, even when taking the possible variation of the nuclear g -factor into account. The treatment for other types of measurements, such as NMR, is less straightforward, and it is not as easily established that we can disentangle them from the HFS measurements. Since this is the case for bismuth, our constraints are only a projection assuming the above treatment gives the same bounds, i.e., a Zeeman measurement yields the same result as the NMR measurement.

Current & projected sensitivities. – Aside from existing sensitivities derived from theoretical and experimental errors, we also give projected bounds. To this end, we spot possible improvements in theoretical calculations with regard to the realistically attainable relative precision, and apply them to the elements in question. Up to now, a complete calculation of the specific difference for heavy HCI is only available for ^{209}Bi [52]. The relative uncertainties on the theory values are rather similar for HCI in the range $50 \leq Z \leq 83$ [56, 86]. In this range, the main difference are the effect of the nuclear charge distributions (Breit-Rosenthal (BR) effect [87, 88]) and the nuclear magnetization distributions (BW effect [73]). Their influence increases up to a factor of 10 for heavy HCI such as $^{209}\text{Bi}^{82+,80+}$ compared to, e.g., $^{133}\text{Cs}^{54+,52+}$.

We use the published calculations for the specific difference of ^{209}Bi and the quoted uncertainties shown in Ref. [52] to estimate the possible theory uncertainty for the specific difference of ^{133}Cs , ^{115}In , and ^{131}Xe , which are rather close in nuclear charge. We, therefore, assume the same uncertainties for those isotopes, starting from the one we derive for caesium. In Ref. [52], five sources of uncertainties are listed for the theory value. All have a similar size.

First, there is the uncertainty due to the higher order interelectronic interactions $1/Z^3$ with a relative precision of 5×10^{-5} . There have been new calculations, achieving relative precision below 10^{-6} for $^{133}\text{Cs}^{52+}$ [58]. Therefore, the remaining uncertainty due to the interelectronic interaction is not a relevant contribution to the overall uncertainty, at least relatively speaking.

Contributions from screened QED calculations have a relative uncertainty of 3×10^{-5} [89]. The dominant uncertainty is given by one diagram regarding photon exchange with an additional bound-electron loop that mediates the hyperfine interaction, that has not been

evaluated yet. We expect it to be possible to calculate this remaining diagram, and thereby improve the relative precision of the screened QED contributions by a factor of 3 for the HFS in $^{133}\text{Cs}^{52+}$.

Although the specific difference is constructed in a way that ensures suppression of the BW effect, there is still a remaining contribution due to the BW effect influencing interelectronic interaction contributions [90]. This part is not completely canceled in the specific difference, resulting in a corresponding uncertainty. The contribution of the BW effect in $^{133}\text{Cs}^{54+,52+}$ is a factor of 7 smaller compared to the one in $^{209}\text{Bi}^{82+,80+}$ [56, 86]. Additionally, the attributed uncertainty for the BW effect in $^{133}\text{Cs}^{54+,52+}$ is a factor of three smaller compared to the one for $^{209}\text{Bi}^{82+,80+}$. Therefore, we estimate the remaining uncertainty in the specific difference to be also a factor of three smaller. The estimated relative uncertainty regarding the remaining BW effect in the specific difference in caesium then amounts to 2×10^{-5} .

The remaining uncertainty due to nuclear polarization has been improved by more than a factor of 50 to a relative precision of 4×10^{-7} for the specific difference of ^{209}Bi [91]. We assume a similar relative uncertainty for ^{133}Cs as well.

The nuclear magnetic moment of the nucleus may be determined via a sub ppb precision measurement of the g_F factor in the ground and the excited state [92–94]. Recently, the bound electron g_j factor of $^{118}\text{Sn}^{49+}$ has been successfully measured with a relative precision 5×10^{-10} [95]. With further realistic improvements on the experimental side, we expect a possible precision of the measured g_F factor of 1×10^{-10} . Together with the theoretical shielding calculations [80, 96] this may lead to a nuclear magnetic moment for ^{133}Cs with a relative precision below 5×10^{-6} , which scales similar for the specific difference of ^{133}Cs as well.

Combining the five estimated uncertainties for the theory value of $\Delta' E$ (^{133}Cs), we find that improvements regarding the theoretical precision can be made up to a relative uncertainty of 2×10^{-5} mainly given by the screened QED uncertainty together with the remaining BW uncertainty.

Finally, a possible measurement of E_{HFS} ($^{133}\text{Cs}^{54+}$) and E_{HFS} ($^{133}\text{Cs}^{52+}$) to MHz precision will lead to $\Delta' E$ (^{133}Cs) with a relative precision of 1×10^{-7} on the experimental side. This might eventually be feasible and achievable in the future, since both wavelengths ($1.9 \mu\text{m}$ and $14 \mu\text{m}$) are accessible by adequate lasers.

We assume similar relative theory uncertainties for $\Delta' E$ (^{115}In) and $\Delta' E$ (^{131}Xe), and a similar experimental precision for $\Delta' E$ (^{115}In), since both wavelengths ($1.4 \mu\text{m}$ and $11 \mu\text{m}$) are accessible by adequate lasers, too. This is unfortunately not the case for $\Delta' E$ (^{131}Xe), where the corresponding wavelength of the lithium-like HFS splitting is larger than $20 \mu\text{m}$ strongly limiting accessible lasers. Therefore, to achieve a ~ 1 MHz precision for the two HFS energy measurements remains a challenging task.

Error estimates on our constraints. – Although the methods outlined in this work should provide quite ac-

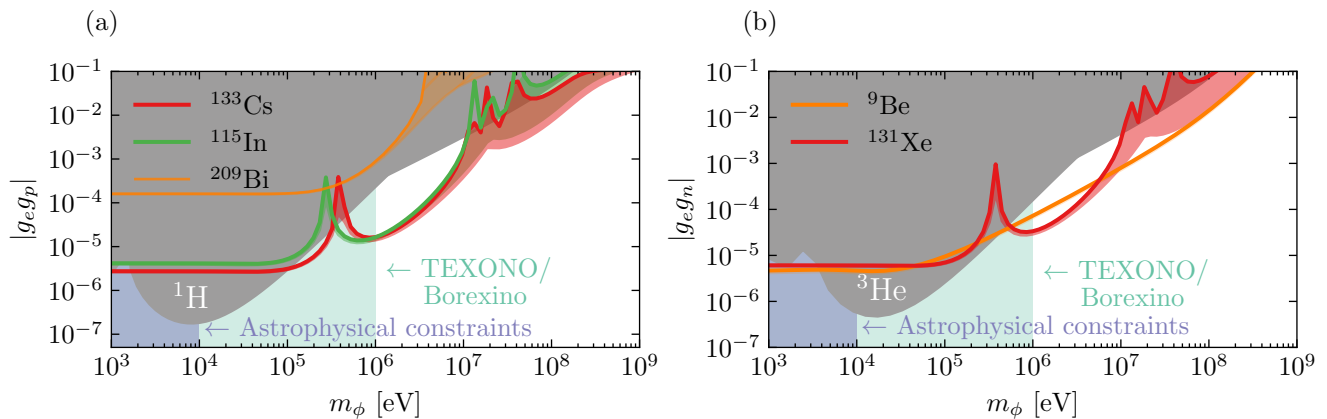


Figure 2. Version of Fig. 1 that includes the error bands (shaded regions) on our constraints/sensitivity projections (solid lines) from our comparison with Ref. [58].

curate results, some care is needed, as the specific differences also lead to subtractions in the signal calculation. Hence, we need to test the sensitivity of our signal calculation to approximation errors.

In principle, further theoretical improvements are possible by accounting for higher orders of interelectronic interactions in the lithium-like system. We can, however, obtain a rough estimate on the uncertainties caused by not including these contributions by comparing our results for the SM hyperfine splitting in lithium-like systems with the ones given in Ref. [58]. We assume that our calculations' error is due to missing diagrams and inaccuracies in our wavefunctions and carry this relative uncertainty over into our calculations for the pseudoscalar-induced hyperfine splitting. Of course, this also implicitly assumes that the relative error is independent of the mass scale in the potential. Since the deviations from literature vary only slowly with Z , we apply the same relative error for elements with a sufficiently similar nuclear charge. We find a relative uncertainty of about 0.1% for mid to high- Z elements, and 1% for low- Z elements.

In Fig. 1, we show the most conservative constraints after incorporating these uncertainties. The corresponding error bands are shown in Fig. 2.

[1] S. G. Karshenboim and V. G. Ivanov, *Phys. Lett. B* **524**, 259–264 (2002).
[2] J. Jaeckel and S. Roy, *Phys. Rev. D* **82** (2010), 10.1103/physrevd.82.125020.
[3] S. G. Karshenboim, *Phys. Rev. D* **82**, 113013 (2010).
[4] F. Ficek, D. F. J. Kimball, M. G. Kozlov, N. Leefer, S. Pustelny, and D. Budker, *Phys. Rev. A* **95**, 032505 (2017).
[5] V. Debierre, C. Keitel, and Z. Harman, *Phys. Lett. B* **807**, 135527 (2020).
[6] G. Adkins, D. Cassidy, and J. Pérez-Ríos, *Phys. Rep.* **975**, 1 (2022).
[7] T. Sailer, V. Debierre, Z. Harman, F. Heiße, C. König, J. Morgner, B. Tu, A. V. Volotka, C. H. Keitel, K. Blaum, and S. Sturm, *Nature* **606**, 479 (2022).
[8] R. M. Potvliege, “Spectroscopy of light atoms and bounds on physics beyond the standard model,”

(2025), [arXiv:2412.16315 \[physics.atom-ph\]](#).
[9] M. Door *et al.*, *Phys. Rev. Lett.* **134** (2025), 10.1103/physrevlett.134.063002.
[10] L. Cong, F. Ficek, P. Fadeev, Y. V. Stadnik, and D. Budker, (2025), [arXiv:2503.07161 \[physics.atom-ph\]](#).
[11] R. M. Potvliege, A. Nicolson, M. P. A. Jones, and M. Spannowsky, *Phys. Rev. A* **108**, 052825 (2023).
[12] K. Wei, W. Ji, C. Fu, A. Wickenbrock, J. Fang, V. V. Flambaum, and D. Budker, *Nat. Comm.* **13**, 7387 (2022), [arXiv:2203.07050 \[physics.atom-ph\]](#).
[13] W. Ji, W. Li, P. Fadeev, F. Ficek, J. Qin, K. Wei, Y.-C. Liu, and D. Budker, *Phys. Rev. Lett.* **130**, 133202 (2023).
[14] K. A. Beyer, I. A. Valuev, C. H. Keitel, M. Tamburini, and N. S. Oreshkina, *Phys. Lett. B* **854**, 138746 (2024), [arXiv:2306.10889 \[hep-ph\]](#).
[15] A. Wilzewski *et al.*, “Nonlinear calcium king plot constrains new bosons and nuclear properties,” (2024), [arXiv:2412.10277 \[physics.atom-ph\]](#).
[16] Z. Xu, X. Heng, G. Tian, D. Gong, L. Cong, W. Ji, D. Budker, and K. Wei, “New constraints on axion mediated dipole-dipole interactions,” (2025), [arXiv:2501.07865 \[hep-ph\]](#).
[17] B. Elder, G. Mentasti, E. Pasatembou, C. F. A. Baynham, O. Buchmueller, C. R. Contaldi, C. de Rham, R. Hobson, and A. J. Tolley, “Prospects for detecting new dark physics with the next generation of atomic clocks,” (2025), [arXiv:2504.07179 \[hep-ph\]](#).
[18] L. Cong *et al.*, (2024), [arXiv:2408.15691 \[hep-ph\]](#).
[19] J. E. Moody and F. Wilczek, *Phys. Rev. D* **30**, 130 (1984).
[20] B. A. Dobrescu and I. Mocioiu, *J. High Energy Phys.* **11**, 005 (2006), [arXiv:hep-ph/0605342](#).
[21] J. E. Kim, *Phys. Rept.* **150**, 1 (1987).
[22] J. Jaeckel and A. Ringwald, *Ann. Rev. Nucl. Part. Sci.* **60**, 405 (2010), [arXiv:1002.0329 \[hep-ph\]](#).
[23] J. Beacham *et al.*, *J. Phys. G* **47**, 010501 (2020), [arXiv:1901.09966 \[hep-ex\]](#).
[24] P. Agrawal *et al.*, *Eur. Phys. J. C* **81**, 1015 (2021), [arXiv:2102.12143 \[hep-ph\]](#).
[25] R. D. Peccei and H. R. Quinn, *Phys. Rev. Lett.* **38**, 1440 (1977).
[26] S. Weinberg, *Phys. Rev. Lett.* **40**, 223 (1978).
[27] J. E. Kim, *Phys. Rev. Lett.* **43**, 103 (1979).
[28] M. A. Shifman, A. I. Vainshtein, and V. I. Zakharov, *Nucl. Phys. B* **166**, 493 (1980).
[29] A. R. Zhitnitsky, *Sov. J. Nucl. Phys.* **31**, 260 (1980).
[30] M. Dine, W. Fischler, and M. Srednicki, *Phys. Lett. B* **104**, 199 (1981).

- [31] L. Di Luzio, M. Giannotti, E. Nardi, and L. Visinelli, *Phys. Rept.* **870**, 1 (2020), [arXiv:2003.01100 \[hep-ph\]](#).
- [32] J. P. Conlon, *J. High Energy Phys.* **05**, 078 (2006), [arXiv:hep-th/0602233](#).
- [33] J. P. Conlon, *Phys. Rev. Lett.* **97**, 261802 (2006), [arXiv:hep-ph/0607138](#).
- [34] A. Arvanitaki, S. Dimopoulos, S. Dubovsky, N. Kaloper, and J. March-Russell, *Phys. Rev. D* **81**, 123530 (2010), [arXiv:0905.4720 \[hep-th\]](#).
- [35] M. Cicoli, M. Goodsell, and A. Ringwald, *J. High Energy Phys.* **10**, 146 (2012), [arXiv:1206.0819 \[hep-th\]](#).
- [36] D. J. E. Marsh, *Phys. Rept.* **643**, 1 (2016), [arXiv:1510.07633 \[astro-ph.CO\]](#).
- [37] B. S. Acharya and C. Pongkitivanichkul, *J. High Energy Phys.* **04**, 009 (2016), [arXiv:1512.07907 \[hep-ph\]](#).
- [38] L. Visinelli and S. Vagnozzi, *Phys. Rev. D* **99**, 063517 (2019), [arXiv:1809.06382 \[hep-ph\]](#).
- [39] I. Broeckel, M. Cicoli, A. Maharana, K. Singh, and K. Sinha, *J. High Energy Phys.* **08**, 059 (2021), [arXiv:2105.02889 \[hep-th\]](#).
- [40] M. Demirtas, N. Gendler, C. Long, L. McAllister, and J. Moritz, (2021), [arXiv:2112.04503 \[hep-th\]](#).
- [41] V. M. Mehta, M. Demirtas, C. Long, D. J. E. Marsh, L. McAllister, and M. J. Stott, *J. Cosmol. Astropart. Phys.* **07**, 033 (2021), [arXiv:2103.06812 \[hep-th\]](#).
- [42] N. Gendler, D. J. E. Marsh, L. McAllister, and J. Moritz, *J. Cosmol. Astropart. Phys.* **09**, 071 (2024), [arXiv:2309.13145 \[hep-th\]](#).
- [43] N. Gendler and D. J. E. Marsh, *Phys. Rev. Lett.* **134**, 081602 (2025), [arXiv:2407.07143 \[hep-th\]](#).
- [44] R. Petrossian-Byrne and G. Villadoro, (2025), [arXiv:2503.16387 \[hep-ph\]](#).
- [45] V. Loladze, A. Platschorre, and M. Reig, (2025), [arXiv:2503.18707 \[hep-ph\]](#).
- [46] J. Preskill, M. B. Wise, and F. Wilczek, *Phys. Lett. B* **120**, 127 (1983).
- [47] L. F. Abbott and P. Sikivie, *Phys. Lett. B* **120**, 133 (1983).
- [48] M. Dine and W. Fischler, *Phys. Lett. B* **120**, 137 (1983).
- [49] P. Arias, D. Cadamuro, M. Goodsell, J. Jaeckel, J. Redondo, and A. Ringwald, *J. Cosmol. Astropart. Phys.* **06**, 013 (2012), [arXiv:1201.5902 \[hep-ph\]](#).
- [50] C. B. Adams *et al.*, “Axion dark matter,” (2023), [arXiv:2203.14923 \[hep-ex\]](#).
- [51] V. M. Shabaev, A. N. Artemyev, V. A. Yerokhin, O. M. Zhrebtssov, and G. Soff, *Phys. Rev. Lett.* **86**, 3959 (2001).
- [52] J. Ullmann *et al.*, *Nat. Comm.* **8** (2017), [10.1038/ncomms15484](#).
- [53] S. Dickopf, B. Sikora, A. Kaiser, M. Müller, S. Ulmer, V. A. Yerokhin, Z. Harman, C. H. Keitel, A. Mooser, and K. Blaum, *Nature* **632**, 757–761 (2024).
- [54] P. Fadeev, Y. V. Stadnik, F. Ficek, M. G. Kozlov, V. V. Flambaum, and D. Budker, *Phys. Rev. A* **99** (2019), [10.1103/physrev.99.022113](#).
- [55] V. M. Shabaev, M. B. Shabaeva, and I. I. Tupitsyn, *Phys. Rev. A* **52**, 3686 (1995).
- [56] V. M. Shabaev, M. Tomaselli, T. Kühl, A. N. Artemyev, and V. A. Yerokhin, *Phys. Rev. A* **56**, 252 (1997).
- [57] A. Schneider, B. Sikora, S. Dickopf, M. Müller, N. S. Oreshkina, A. Rischka, I. A. Valuev, S. Ulmer, J. Walz, Z. Harman, C. H. Keitel, A. Mooser, and K. Blaum, *Nature* **606**, 878–883 (2022).
- [58] V. P. Kosheleva, A. V. Volotka, D. A. Glazov, and S. Fritzsche, *Phys. Rev. Res.* **2**, 013364 (2020).
- [59] G. Breit, *Phys. Rev.* **35**, 1447 (1930).
- [60] D. E. Zwanziger, *Phys. Rev.* **121**, 1128 (1961).
- [61] J. R. Sapirstein, *Phys. Rev. Lett.* **51**, 985 (1983).
- [62] T. Schmidt, *Z. Phys.* **106**, 358–361 (1937).
- [63] L. Leimenstoll, *Constraining new pseudoscalar bosons using atomic spectroscopy*, Bachelor’s thesis (2024).
- [64] V. A. Dzuba, V. V. Flambaum, I. B. Samsonov, and Y. V. Stadnik, *Phys. Rev. D* **98** (2018), [10.1103/physrevd.98.035048](#).
- [65] M. E. Rose and W. H. Furry, *Am. J. Phys.* **29**, 866 (1961).
- [66] G. W. F. Drake, *Springer Handbook of Atomic, Molecular, and Optical Physics* (2006).
- [67] J. Sapirstein and K. T. Cheng, *Phys. Rev. A* **63**, 032506 (2001).
- [68] N. S. Oreshkina, D. A. Glazov, A. V. Volotka, V. M. Shabaev, I. I. Tupitsyn, and G. Plunien, *Phys. Lett. A* **372**, 675 (2008).
- [69] W. Kohn and L. J. Sham, *Phys. Rev.* **140**, A1133 (1965).
- [70] P. Hohenberg and W. Kohn, *Phys. Rev.* **136**, B864 (1964).
- [71] J. Sapirstein and K. T. Cheng, *Phys. Rev. A* **67**, 022512 (2003).
- [72] W. Johnson, *Atomic Structure Theory* (Springer Berlin, Heidelberg, 2007).
- [73] A. Bohr and V. F. Weisskopf, *Phys. Rev.* **77**, 94 (1950).
- [74] S. Boucard and P. Indelicato, *Eur. Phys. J. D* **8**, 59 (2000).
- [75] L. Cong, F. Ficek, P. Fadeev, and D. Budker, (2024), [arXiv:2408.11009 \[physics.atom-ph\]](#).
- [76] I. Kuzmenko, T. Kuzmenko, Y. Avishai, and Y. B. Band, *Phys. Rev. A* **108**, 052804 (2023).
- [77] H. M. Chang, H. T. Wong, M. H. Chou, M. Deniz, H. X. Huang, F. S. Lee, H. B. Li, J. Li, H. Y. Liao, S. T. Lin, V. Singh, S. C. Wu, and B. Xin, *Physical Review D* **75** (2007), [10.1103/physrevd.75.052004](#).
- [78] D. Basilico *et al.* (BOREXINO), (2025), [arXiv:2504.19135 \[hep-ex\]](#).
- [79] S. G. Karshenboim, *Phys. Rep.* **422**, 1 (2005).
- [80] V. A. Yerokhin, K. Pachucki, Z. Harman, and C. H. Keitel, *Phys. Rev. Lett.* **107**, 043004 (2011).
- [81] V. A. Yerokhin, K. Pachucki, Z. Harman, and C. H. Keitel, *Phys. Rev. A* **85**, 022512 (2012).
- [82] P. Carenza and G. Lucente, *Phys. Rev. D* **103** (2021), [10.1103/physrevd.103.123024](#).
- [83] A. Lella, P. Carenza, G. Co’, G. Lucente, M. Giannotti, A. Mirizzi, and T. Rauscher, *Phys. Rev. D* **109**, 023001 (2024).
- [84] W. Johnson and G. Soff, *At. Data Nucl. Data Tables* **33**, 405 (1985).
- [85] V. M. Shabaev, *Phys. Rep.* **356**, 119–228 (2002).
- [86] V. M. Shabaev, M. B. Shabaeva, I. I. Tupitsyn, V. A. Yerokhin, A. N. Artemyev, T. Kühl, M. Tomaselli, and O. M. Zhrebtssov, *Phys. Rev. A* **57**, 149 (1998).
- [87] J. E. Rosenthal and G. Breit, *Phys. Rev.* **41**, 459 (1932).
- [88] M. F. Crawford and A. L. Schawlow, *Phys. Rev.* **76**, 1310 (1949).
- [89] O. V. Andreev, D. A. Glazov, A. V. Volotka, V. M. Shabaev, and G. Plunien, *Phys. Rev. A* **85**, 022510 (2012).
- [90] O. M. Zhrebtssov and V. M. Shabaev, *Can. J. of Phys.* **78**, 701 (2000), [https://doi.org/10.1139/p00-060](#).
- [91] A. V. Volotka and G. Plunien, *Phys. Rev. Lett.* **113**, 023002 (2014).
- [92] W. Quint, D. L. Moskovkin, V. M. Shabaev, and M. Vogel, *Phys. Rev. A* **78**, 032517 (2008).
- [93] F. Herfurth and others for the HITRAP collaboration, *Phys. Scr.* **2015**, 014065 (2015).
- [94] M. Vogel *et al.*, *Phys. Scr.* **2015**, 014066 (2015).
- [95] J. Morgner *et al.*, *Nature* **622**, 53 (2023).
- [96] D. L. Moskovkin, N. S. Oreshkina, V. M. Shabaev, T. Beier, G. Plunien, W. Quint, and G. Soff, *Phys. Rev. A* **70**, 032105 (2004).